Two-dimensional electron momentum distribution of graphite

1991 J. Phys.: Condens. Matter 3 1699

(http://iopscience.iop.org/0953-8984/3/12/002)

J. Phys.: Condens. Matter 3 (1991) 1699–1707. Printed in the UK

Two-dimensional electron momentum distribution of graphite

Lou Yongming†‡, *B Johansson*† *and R M Nieminen*§

† Condensed Matter Theory Group, Physics Department, Uppsala University, Box 530, S-75121, Uppsala, Sweden

‡ Physics Department, Tsinghua University, Beijing, People's Republic of China

§ Laboratory of Physics, Helsinki University of Technology, SF-02150 Espoo, Finland

Received 27 April 1990

Abstract. Using the empirical pseudopotential method, we have calculated the Compton profiles and the two-dimensional electron momentum distribution (EMD) for graphite. The calculated Compton profiles as well as their anisotropy are in good agreement with experiments and compare well with other theoretical calculations. Although the anisotropy of the directional Compton profile (one-dimensional EMD) is small, the two-dimensional electron momentum distribution shows a large anisotropy, and a layer structure is found in the two-dimensional EMD integrated over the c axis. It is shown that the layer structure is more clearly exhibited by the two dimensional EMD than by the one-dimensional EMD (Compton profile).

1. Introduction

The electronic structure of graphite has been studied intensively in recent years [1–22]. This interest is partly due to the fact that graphite can be considered as a prototype for quasi-two-dimensional materials. For relatively recent reviews of the electronic energy band structure of graphite the reader is referred to references [1] and [2]. While the occupied energy band structure has been established experimentally by angle-resolved photoemission spectroscopy [8–13] and found to be in good agreement with the theoretical work [1–7], the unoccupied band structure is still a matter of discussion both theoretically and experimentally [21]. The recent experiments of angle-resolved inverse photoemission spectroscopy (ARIPES) [21, 22] on single-crystal graphite showed some disagreement between the theoretical conduction bands and the experimental data.

Compton scattering of x- and γ-rays has been successfully applied to determine the electron momentum distribution (EMD) of several materials [23, 24]. Also for graphite, the Compton profile has been measured and calculated by a number of groups [25–33] in order to investigate the EMD and its anisotropy. Since a large single crystal of graphite has not been available until relatively recently, all the previous measurements of Compton profiles had to be carried out on samples of highly oriented pyrolytic graphite (HOPG). The nature of HOPG is such that the c axis is highly oriented while the xy direction (in the basal plane) is completely random. Thus the experiments can only measure the profiles along the c axis and an average within the xy plane. Furthermore, each measurement is also somewhat averaged around the c axis due to the mosaic spread of

0953-8984/91/121699 + 09 $03.50

the HOPG sample. The measured anisotropy is considerably smaller than what one would at first expect from the layer structure of graphite and is also smaller than the anisotropy of the corresponding angular correlation distribution in positron annihilation experiments [34, 35]. There are several reasons for these small anisotropies of the Compton profile. Among them, the mosaic spread causes a substantial reduction of the anisotropy of the profile [32], which will be discussed in detail in section 3.

Due to the fact that the Compton profile can only measure the one-dimensional electron momentum distribution, all previous theoretical calculations on graphite have dealt with the one-dimensional EMD. In the last decade, the positron annihilation technique has developed rapidly [36]. The two-dimensional angular correlation distribution of the electron-positron annihilation (ACAR) has become well established as a tool to investigate the electron momentum distribution [36]. Interestingly enough the two-dimensional ACAR of graphite shows a strong anisotropy [37]. Since the ACAR is closely related to the EMD, it is our purpose to investigate whether or not a higher dimensional EMD than the one-dimensional EMD (Compton profile) also shows a strong anisotropy similar to the corresponding ACAR. In the present study, we will concentrate on the anisotropy of the electron momentum distribution. Using the electron wavefunction calculated from the empirical pseudopotential method (EPM) we have calculated both the one-dimensional EMD (Compton profile) and the two-dimensional EMD. Our one-dimensional EMD shows, in general, a good agreement with both the experimental data and earlier theoretical calculations. Below we will demonstrate that the layer structure of graphite can be more easily understood by means of the two-dimensional EMD than the one-dimensional EMD.

2. Theoretical calculations

When only the electron momentum distribution is required, the pseudopotential method has some advantages relative to other methods, such as that the calculated wavefunction has the full point symmetry of the crystal and no Fourier transformation is needed. These advantages are of course lost for cases in which this method does not give a reasonable description of the ground state band structure. As will be discussed below, in the present case of graphite the pseudopotential method does give a reasonable description of the occupied bands, and therefore we can confidently use this method in the present work. The pseudopotential formalism has become a well established method of investigating the electronic structure of s–p bonded materials [38, 39]. The reader is referred to [38] and [39] for details of the formalism. Van Haeringen and Junginger [40] have used this method to calculate the energy band of graphite and their overall results are in reasonably good agreement with experiment. Holzwarth *et al* [2] have also used the pseudopotential technique and the local density functional approximation together with a mixed basis set of plane waves and linear combinations of atomic orbitals to calculate the energy bands of graphite. The results of the occupied bands in graphite are in good agreement with other calculations and with angle-resolved photoemission experiments [8]. The unoccupied band structure is closer to the experiments of ARIPES than other previous calculations although some disagreement still exists between the calculation and experimental data [21, 22]. We choose the pseudopotential form factor parameters from curve 1 in [28] to calculate the electron wavefunction. The calculated energy bands are in general good agreement with the theoretical result of [2], and the Compton profile

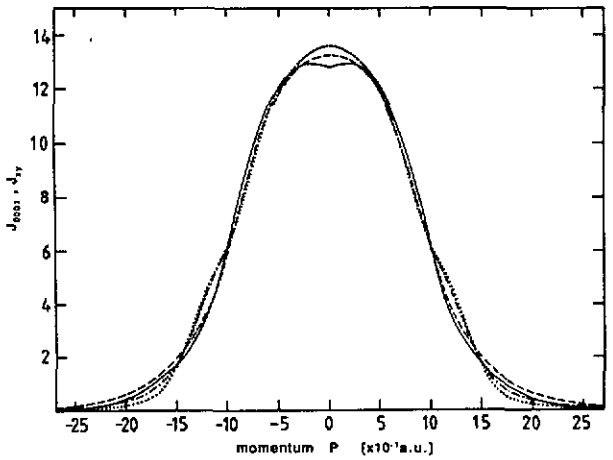

Figure 1. Directional Compton profiles for graphite. The dotted curve and the full curve are the present calculations. The chain curve and broken curve are the results from [33]. The dotted curve and chain curve represent the J_{xy} profile averaged over the xy basal plane. The broken curve and the full curve represent the J_{0001} profile along the [0001] direction.

compares well with the theoretical results of Chou *et al* [33] which will be discussed in detail in section 3.

The EMD is given by

$$\rho(\boldsymbol{p}) = \sum_{n,k}^{\text{all}} f(E_{n,k}) \left| \int \mathrm{d}\boldsymbol{r} \exp(-\mathrm{i}\boldsymbol{p}\cdot\boldsymbol{r})\Psi_{n,k}(\boldsymbol{r}) \right|^2 \tag{1}$$

where $\Psi_{n,k}$ is the electron wavefunction for an electron in the nth band with wave vector $\boldsymbol{k}$ inside the first Brillouin zone, and $f(E_{n,k})$ is the Fermi–Dirac distribution function. The electron wavefunction can be expanded as

$$\Psi_{n,k}(\boldsymbol{r}) = \sum_{G}^{\text{all}} C_{n,-G}(\boldsymbol{k}) \exp[\mathrm{i}(\boldsymbol{k}-\boldsymbol{G})\cdot\boldsymbol{r}] \tag{2}$$

where $\boldsymbol{G}$ is the reciprocal lattice vector. We then obtain

$$\rho(\boldsymbol{p}) = \sum_{n,k}^{\text{all}} f(E_{n,k}) \sum_{G}^{\text{all}} |C_{n,-G}(\boldsymbol{k})|^2 \, \delta(\boldsymbol{k}-\boldsymbol{p}-\boldsymbol{G}). \tag{3}$$

In our calculations we have included 581 reciprocal lattice vectors in the summation of equations (2) and (3). The two-dimensional EMD is obtained from

$$I(p_x, p_y) = \int \rho(\boldsymbol{p}) \, \mathrm{d}p_z. \tag{4}$$

Using the impulse approximation, the Compton profile, $J(p_z)$, is simply the projection of $\rho(\boldsymbol{p})$ along the scattering vector [24]

$$J(p_z) = \iint \rho(\boldsymbol{p}) \, \mathrm{d}p_x \, \mathrm{d}p_y. \tag{5}$$

3. Results and discussion

In figure 1 we show the calculated profile J_{0001} along the c-axis [0001] direction and also the profile J_{xy} averaged over the xy basal plane and compare them with corresponding

Table 1. Calculated valence-electron Compton profile along two symmetry directions for graphite.

p (au)	[0001]	xy
0.0	1.905	2.021
0.1	1.919	2.011
0.2	1.923	1.983
0.3	1.912	1.935
0.4	1.870	1.867
0.5	1.794	1.772
0.6	1.683	1.642
0.7	1.533	1.465
0.8	1.359	1.256
0.9	1.152	1.064
1.0	0.922	0.910
1.1	0.691	0.808
1.2	0.528	0.684
1.3	0.409	0.538
1.4	0.325	0.382
1.5	0.258	0.240
1.6	0.202	0.144
1.7	0.156	0.085
1.8	0.120	0.057
1.9	0.090	0.041
2.0	0.064	0.030
2.1	0.044	0.023
2.2	0.030	0.018
2.3	0.021	0.015
2.4	0.015	0.012
2.5	0.011	0.010

theoretical profiles [33]. In the latter work a linear combination of atomic orbitals, which was not included in our calculation, was used together with plane waves. Therefore the contribution from the core region in [33] is larger than the one in the present calculation. In addition, the pseudo-wavefunctions do not have oscillations near the nuclei, therefore the amplitude of the presently calculated Compton profile at large momenta is expected to be smaller than both the experimental profile and that of an all-electron calculation. In order to remove the small and smooth contributions due to the core part of the wavefunction, the profiles J_{xy} have been normalized to have a same value at $p = 0$. Our results are in general agreement with the calculations of [33], especially for the profile J_{xy} averaged over the basal plane. The small difference between the two calculations is most likely due to the different basis set employed in the calculations. Unfortunately the most recent experimental Compton profiles [31, 32] are not available in tabular form in the literature. However since the theoretical profiles in [33] are in excellent agreement with experimental data, it is sufficient to compare our results with their calculations. For convenience we also list the values of the calculated profiles along the two directions for graphite in table 1. The profile is normalized in such a way that, when integrated from $-\infty$ to $+\infty$, it gives the number of valence electrons (4). The indirect comparison of our results with the experiment, through the theoretical profile in [33], therefore shows that our results are in general agreement with experiment. The remaining difference between

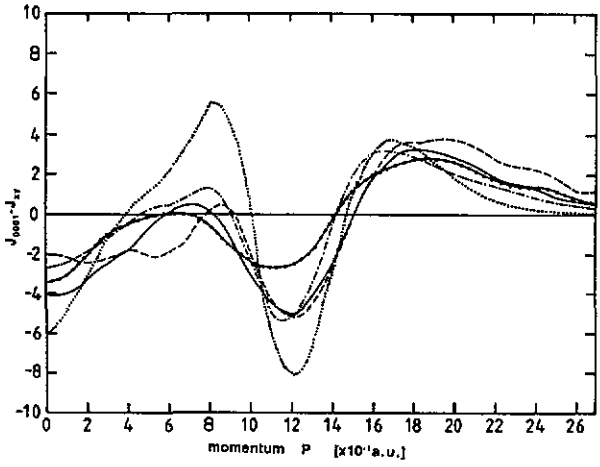

Figure 2. Compton-profile anisotropy $J_{0001}-J_{xy}$ for graphite. The dotted curve is the present calculation and the chain curve is the calculation from [33]. The broken curve is the measurement from [30] and the full curve is the measurement from [31]. The curve with solid circles is the measurement from [32]. The present theoretical curve has not been smeared for the effects of mosaic spread, experimental resolution, and annular source geometry.

our present calculations and the experimental profiles can be reduced through the following procedures:

(i) optimizing the pseudopotential parameters;

(ii) including the electron–electron many-body correction suggested by Bauer *et al* [41, 42]; and

(iii) using a single crystal of graphite in the Compton experiment.

The optimization of the potential parameters is, however, very computer time consuming due to the big unit cell of graphite which requires a large number of reciprocal lattices vectors G and many potential parameters in the calculation. Concerning point (iii) it would be of great help if a variety of experimental data were available for single crystal graphite instead of HOPG. At present there are only a few experiments, such as ARIPES measurements [21, 22], performed on single crystal graphite.

The calculated Compton-profile anisotropy and the measured anisotropy profiles from [30–32] together with the theoretical results from [33] are shown in figure 2. The present theoretical Compton-profile anisotropy is in general good agreement with the experimental data [30–32] and also compares well with the other theoretical calculations [33]. Our anisotropic profile is found to be larger in the lower momentum region ($p < 1.4$ au) and smaller in the higher momentum region ($p > 1.7$ au) than the experimental data. This difference can be understood from the following discussion. Firstly, the pseudopotential method used in the present calculation does not consider the core electron contribution. This means that the amplitude of the calculated Compton profile at large momenta is smaller than that obtained from an all-electron calculation and the experimental data. The potential parameters we actually have employed may also be somewhat smaller than the real potential parameters. Secondly, the lack of a large single crystal of graphite, as discussed above, has led to the use of HOPG in the experiment. This causes each measurement to be somewhat averaged around the c-axis and reduces the anisotropy of the directional profile due to the mosaic spread of the HOPG sample. In [32] it was shown that a 53° mosaic spread of the graphite sample used in the experiment reduces the maxima and minima of the anisotropy by 25%. Besides, the effects of the experimental resolution and the annular source geometry will also reduce the anisotropy of the profile [32]. Since in the future large size single crystals of graphite will become

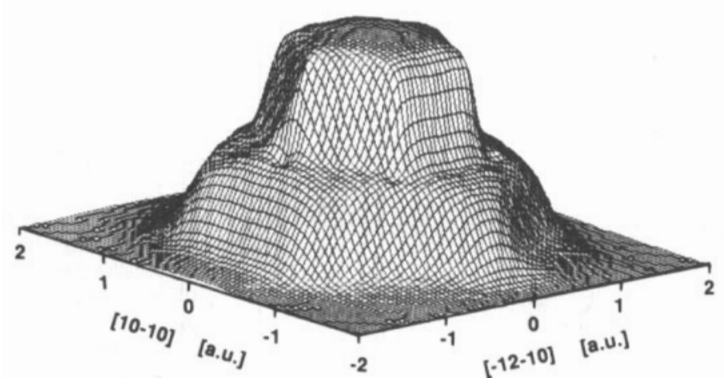

Figure 3. The two-dimensional electron momentum distribution $I(p_x, p_y)$ of graphite integrated along the [0001] direction. $p_x \| [10-10]$ and $p_y \| [-12-10]$.

available, we have chosen not to smear our theoretical profile for the effects of mosaic spread, experimental resolution, and annular source geometry in order to facilitate future comparisons with new experimental data.

Our main purpose in the present work is to see whether or not the higher dimensional EMD shows a larger anisotropy in analogy to what has been observed in positron experiments [37]. The comparison above between our present results, experimental data and the theoretical calculations in [33] shows that our one-dimensional EMD is a good approximation. Having this confidence in our results we proceed to investigate higher dimensional EMD. In figure 3 we show the two-dimensional EMD integrated along the c-axis [0001] direction. The layer structure can now be clearly seen. In the central part of the Brillouin zone, the amplitude of the two-dimensional EMD is almost constant and has hexagonal symmetry. Near the first Brillouin zone faces $\langle 10-10 \rangle$, the amplitude of the two-dimensional EMD drops sharply to about its half-maximum value. For semimetals, semiconductors or insulators this might be a typical feature of layer structures with large layer separations. The central plateau in the distribution is caused by a strong potential parameter along the c-axis direction which gives rise to a strong correlation between the wavefunctions with wave vector $\boldsymbol{k}$ in the first Brillouin zone and with wave vector $\boldsymbol{G}_{\langle 0002 \rangle} - \boldsymbol{k}$ in the higher zone directly above or below the first Brillouin zone, i.e. $\Psi(\boldsymbol{k})$ and $\Psi(\boldsymbol{G}_{\langle 0002 \rangle} - \boldsymbol{k})$. The sharp drop of the distribution is caused by the strong correlation between the wavefunction $\Psi(\boldsymbol{k})$ and the wavefunction $\Psi(\boldsymbol{G}_{\langle 10-10 \rangle} - \boldsymbol{k})$ near the Bragg plane $\boldsymbol{G}_{\langle 10-10 \rangle}/2$. If the layer spacing c is small, the corresponding potential parameters $U(\boldsymbol{G})$, with $\boldsymbol{G}$ along the [0001] direction, will also be small and there will not be such a feature, i.e. the plateau in the central part of the Brillouin zone and the sharp drop near the first Brillouin zone face $\boldsymbol{G}_{\langle 10-10 \rangle}/2$ in the two-dimensional EMD. To investigate this we have adjusted the potential parameters to see whether or not this feature will disappear. In all the calculations we find that it remains present. We therefore expect that graphite might not be a unique case for having such a layer structure in its two-dimensional EMD. It would be interesting to see whether the corresponding two-dimensional ACAR integrated along [0001] has a similar shape, since it can also be measured.

Another two-dimensional EMD integrated along the [10 − 10] direction is shown in figure 4. The distribution is nearly of bimodal form with a saddle point at $(p_{-12-10}, p_{0001}) =$

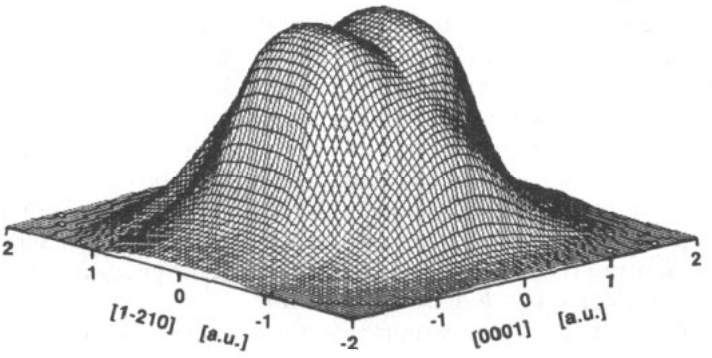

Figure 4. The two-dimensional electron momentum distribution $I(p_y, p_z)$ of graphite integrated along the [10 − 10] direction. $p_y \| [1 - 210]$ and $p_z \| [0001]$.

(0, 0) which is similar to the observations in the corresponding distribution of the positron–electron annihilation experiment in graphite [37] but has a broader distribution and a more shallow valley at the center of the EMD. Unlike the two-dimensional EMD integrated along the [0001] direction, the two-dimensional EMD integrated along the [10 − 11] direction is quite dependent on the potential parameters. When adjusting the potential parameters, there were cases when the bimodal shape disappeared. This bimodal distribution should be tested by calculation using a different formalism. It can also be tested experimentally by the two-dimensional reconstruction from the directional Compton profiles measured from a single crystal of graphite. It is known that the contribution of the core electrons to the electron momentum distribution, which is not included in the present pseudopotential calculation, is considerably smoother than the contribution from the valence and conduction electrons. Therefore, the bimodal shape in the two-dimensional EMD should be present from the reconstruction of the directional Compton profiles measured from a single crystal of graphite, despite the fact that there will be a small amount of core electron contributions which can not be separated from the valence and conduction electron contributions. It is hoped that the two-dimensional EMD will be useful in the future study of graphite as well as of the other layer structure materials.

Similar to the Compton profile, the ACAR of the positron–electron annihilation also provides information about the EMD. While the experimental results for diamond reveal only a small difference between the two types of measurement, in graphite the differences are extremely large [26]. Perhaps this is one of the largest differences between the two types of measurements for s–p bonded materials. The anisotropy in the ACAR is much larger than in the Compton profile. In addition the ACAR distribution is much narrower than the Compton profile. These differences for graphite between the Compton profiles and the ACAR of positron annihilation arise from the following reasons:

(i) the Coulomb perturbation on the wavefunction of the annihilated electron by the positron [34, 35, 37];

(ii) the positron preferring to stay in the interlayer region, where the electron density is lower and the local electron momentum distribution is narrower than the averaged bulk values;

(iii) The details of the positron wavefunction [34, 35, 37].

The Coulomb perturbation of the positron on the electron wavefunction is rather difficult to deal with because the effective density of the delocalized positron will be nearly zero due to there being only one single positron present. Since the positron prefers to stay in the interlayer region, it will tend to favour annihilation with π electrons than with σ electrons. It is known that the EMD of σ electrons is quite isotropic, while the EMD of π electrons is highly anisotropic. The preferential annihilation of the positron with the π electron is the reason for the anisotropy of the ACAR being more pronounced than it is for the Compton profile. For the same reason i.e., the preferential annihilation in the interlayer region and the narrow local EMD in the interlayer region, the ACAR is much narrower than the corresponding Compton profile.

Like the Compton profile measurements, the positron experiments suffer from the lack of large single crystals of graphite. It is found, using a sample stacked by four fairly good single crystals, that the measured two-dimensional ACAR [43] is markedly different than the results [37] from the HOPG sample. At present, data are not available for the two-dimensional ACAR integrated along [0001] direction. Such data might, however, soon become available together with other differently oriented two-dimensional ACAR measurements from higher quality single crystal samples than have been used previously [44]. It would be valuable if the Compton profile and the ACAR of the positron annihilation were studied jointly on the same sample and if the reconstruction two-dimensional and three-dimensional EMD from Compton profile and the three-dimensional reconstruction ACAR from the two-dimensional ACAR could be done together. This would provide a unique understanding of the EMD as well as the electron wavefunction for graphite, and perhaps of other layer structure materials too. Further work on the ACAR of the positron annihilation is in progress and will be discussed elsewhere.

4. Conclusion

We have calculated the directional Compton profiles of graphite and the corresponding anisotropy profiles. Our results are in general agreement with experimental data and other theoretical calculations. We have also calculated the two-dimensional electron momentum distribution and propose a way of verifying these two-dimensional distributions. It is shown that although the directional Compton profile (one-dimensional EMD) of graphite is only weakly anisotropic, the two-dimensional EMD shows a large anisotropy. The layer structure of graphite could be more easily understood by its two-dimensional EMD or the two-dimensional reconstruction of the Compton profiles than by the Compton profile itself. The experimental ACAR of positron annihilation is compared with the Compton profile and the EMD. The new features of the two-dimensional EMD together with its relation to the corresponding ACAR of positron experiments deserve further investigations for graphite as well as other layer structure materials.

Acknowledgments

Lou Yongming and B Johansson would like to acknowledge the Swedish Natural Science Research Council (NFR) for financial support.

References

[1] Tatar R C and Rabii S 1982 *Phys. Rev.* B **25** 4126
[2] Holzwarth N A W, Louie S G and Rabii S 1982 *Phys. Rev.* B **26** 5382
[3] Mallet C P 1981 *J. Phys. C: Solid State Phys.* **14** L213
[4] Zunger A 1978 *Phys. Rev.* B **17** 626
[5] Willis R F, Fitton B and Painter G S 1974 *Phys. Rev.* B **9** 1926
[6] Posternak M, Balderschi A, Freeman A J, Wimmer E and Weinert M 1983 *Phys. Rev. Lett.* **50** 761
[7] Posternak M, Balderschi A, Freeman A J and Wimmer E 1984 *Phys. Rev. Lett.* **52** 863
[8] Eberhardt W, McGovern I T, Plummer E W and Fischer J E 1980 *Phys. Rev. Lett.* **44** 200
McGovern I T, Eberhardt W, Plummer E W and Fischer J E 1980 *Physica* B **99** 415
[9] Law A R, Barry J J and Hughes H P 1983 *Phys. Rev.* B **28** 5332
[10] Marchand D, Frétigny C, Laguës M, Batallan F, Simon Ch, Rosenman I and Pinchaux R 1984 *Phys. Rev.* B **30** 4788
[11] Law A R, Johnson M T and Hughes H P 1986 *Phys. Rev.* B **34** 4289
[12] Pescia D, Law A R, Johnson M T and Hughes H P 1985 *Solid State Commun.* **56** 809
[13] Takahashi T, Tokailin H and Sagawa T 1985 *Phys. Rev.* B **32** 8317
[14] Law A R, Johnson M T, Hughes H P and Padmore H A 1985 *J. Phys. C: Solid State Phys.* **18** L297
Johnson M T, Law A R and Hughes H P 1985 *Surf. Sci.* **162** 11
[15] Papagno L and Caputi L S 1983 *Surf. Sci.* **125** 530
[16] Fauster Th, Himpsel F J, Fisher J E and Plummer E W 1983 *Phys. Rev. Lett.* **51** 430
[17] Reihl B, Gimzewski J K, Nicholls J M and Tosatti E 1986 *Phys. Rev.* B **33** 5770
[18] Schäfer I, Schüter M and Skibowski M 1987 *Phys. Rev.* B **35** 7663
[19] Ohsawa H, Takahashi T, Kinoshita T, Enta Y, Ishii H and Sagawa T 1987 *Solid State Commun.* **61** 347
Maeda F, Takahashi T, Ohsawa H and Suzuki S 1988 *Phys. Rev.* B **37** 4482
[20] Dittmar-Wituski A, Naparty M and Skonieczny J 1985 *J. Phys. C: Solid State Phys.* **18** 2563
[21] Claessen R, Carstensen H and Skibowski M 1988 *Phys. Rev.* B **38** 12582
[22] Collins I R, Andrews P T and Law A R 1988 *Phys. Rev.* B **38** 13348
[23] Williams B G ed 1977 *Compton Scattering* (New York: McGraw-Hill)
[24] Cooper M J 1985 *Rep. Prog. Phys.* **48** 415
[25] Cooper M and Leake J A 1967 *Phil. Mag.* **5** 1201
[26] Weies R J and Phillips W C 1968 *Phys. Rev.* **176** 900
[27] Paakkari T L P 1974 *Phys. Fenn.* **9** 185
[28] Reed W A, Eisenberger P, Pandey K C and Snyder L C 1974 *Phys. Rev.* **10** 1507
[29] Dovesi R, Pisani C, Roetti C and Dellarole 1981 *Phys. Rev.* B **24** 4170
[30] Vasudevan S, Rayment T, Williams B G and Holt R 1984 *Proc. R. Soc.* A **391** 109
[31] Loupias G, Chomilier J and Guérard D 1984 *J. Physique Lett.* **45** L301; 1985 *Solid State Commun.* **55** 299
[32] Tyk R, Felsteiner J, Gertner I and Moreh R 1985 *Phys. Rev.* B **32** 2625
[33] Chou M Y, Cohen Marvin L and Louie Steven G 1986 *Phys. Rev.* B **33** 6619
[34] Berko S, Kelley R E and Plaskett J S 1957 *Phys. Rev.* **106** 824
[35] Cartier E, Heinrich F, Gubler U M, Pfluger P, Geiser V and Güntherodt H-J 1983 *Synthetic Metals* **8** 119
[36] See, for example Berko S 1983 *Positron Solid State Physics* ed W Brandt and A Dupasquier (New York: North Holland) p 64
Mijnarends P E 1983 *Positron Solid State Physics* ed W Brandt and A Dupasquier (New York: North Holland) p 146
[37] Lee R R, von Stetter E C, Hasegawa M and Berko S 1987 *Phys. Rev. Lett.* **58** 2363
[38] Harrison W A ed 1966 *Pseudopotentials in The Theory of Metals* (New York: Benjamin)
[39] Ehrenreich H, Seitz F and Turnbull D ed 1970 *Solid State Physics 24* (New York: Academic)
[40] van Haeringen W and Junginger H G 1969 *Solid State Commun.* **7** 1723
[41] Bauer G E W 1983 *Phys. Rev.* B **27** 5912
[42] Bauer G E W and Schneider J R 1983 *Solid State Commun.* **47** 673; 1984 *Phys. Rev. Lett.* **52** 2061; 1984 *J. Phys. Chem. Solid* **45** 675; 1985 *Phys. Rev.* B **31** 681
[43] Kanazawa I, Tanigawa S, Suzuki R, Mizuhara Y, Sano M and Inokuchi H 1987 *J. Phys. Chem. Solids* **48** 701
[44] Tanigawa S private communication